Nuclear Materials and Energy 9 (2016) 75–83

Contents lists available at ScienceDirect

Nuclear Materials and Energy

journal homepage: www.elsevier.com/locate/nme

Chemically deposited tungsten fibre-reinforced tungsten – The way to a mock-up for divertor applications

J. Riesch[a,*], M. Aumann[b], J.W. Coenen[b], H. Gietl[a], G. Holzner[a], T. Höschen[a], P. Huber[c], M. Li[a], Ch. Linsmeier[b], R. Neu[a,d]

[a] Max-Planck-Institut für Plasmaphysik, 85748 Garching, Germany
[b] Forschungszentrum Jülich GmbH, Institut für Energie- und Klimaforschung – Plasmaphysik, Partner of the Trilateral Euregio Cluster (TEC), 52425 Jülich, Germany
[c] Institut für Textiltechnik (ITA) der RWTH Aachen University, 52072 Aachen, Germany
[d] Technische Universität München, 85748 Garching, Germany

ARTICLE INFO

Article history:
Received 28 December 2015
Revised 16 March 2016
Accepted 17 March 2016
Available online 4 May 2016

Keywords:
Tungsten
Fibre-reinforced composite
Mock-up
Divertor
Chemical vapour deposition

ABSTRACT

The development of advanced materials is essential for sophisticated energy systems like a future fusion reactor. Tungsten fibre-reinforced tungsten composites (W_f/W) utilize extrinsic toughening mechanisms and therefore overcome the intrinsic brittleness of tungsten at low temperature and its sensitivity to operational embrittlement. This material has been successfully produced and tested during the last years and the focus is now put on the technological realisation for the use in plasma facing components of fusion devices. In this contribution, we present a way to utilize W_f/W composites for divertor applications by a fabrication route based on the chemical vapour deposition (CVD) of tungsten. Mock-ups based on the ITER typical design can be realized by the implementation of W_f/W tiles. A concept based on a layered deposition approach allows the production of such tiles in the required geometry. One fibre layer after the other is positioned and ingrown into the W-matrix until the final sample size is reached. Charpy impact tests on these samples showed an increased fracture energy mainly due to the ductile deformation of the tungsten fibres. The use of W_f/W could broaden the operation temperature window of tungsten significantly and mitigate problems of deep cracking occurring typically in cyclic high heat flux loading. Textile techniques are utilized to optimise the tungsten wire positioning and process speed of preform production. A new device dedicated to the chemical deposition of W enhances significantly, the available machine time for processing and optimisation. Modelling shows that good deposition results are achievable by the use of a convectional flow and a directed temperature profile in an infiltration process.

1. Introduction

The so called DEMOnstration power plant DEMO will be the first fusion reactor producing electricity and is therefore the next step towards realizing fusion based energy systems [1,2]. If considering such a fusion based power plant a combination of multiple issues needs to be evaluated [3,4]. Currently such a reactor only exists in the form of early design studies where detailed operational requirements are just now being developed [5,6].

For the first wall material of DEMO unique challenges require complex features in areas ranging from mechanical strength to thermal properties. The main challenges include wall lifetime, erosion, fuel management and overall safety. For the lifetime of the wall material, considerations of thermal fatigue as well as transient heat loading are crucial as typically 1×10^9 (30 Hz) thermal transients (ELMs) during one full power year of operation are to be expected. For next step devices, limits on power exhaust, availability and lifetime are far more restraint than for current research-use-only reactors [6]. The development of advanced materials especially having high temperature strength and high fracture resistance/damage tolerance is therefore essential for a future fusion power plant [7].

Tungsten (W) is currently the main candidate material for the first wall of a fusion reactor due to its unique property combination e.g. the high melting point and the high temperature strength as well as an excellent erosion resistance and a low

* Corresponding author.
E-mail address: johann.riesch@ipp.mpg.de (J. Riesch).

http://dx.doi.org/10.1016/j.nme.2016.03.005

tritium retention [7]. For this reasons a solution based on actively cooled tungsten components has been developed for the divertor of the next generation device, ITER [8].

However, as a typical bcc metal, tungsten exhibits a so called ductile-to-brittle transition (DBT) [9]. Below a certain temperature, the DBT temperature (DBTT), these materials show brittle behaviour. The transition temperature is very much dependent on the composition, the fabrication process, and the pre-treatment as well as the testing method. It lies typically between 500 K and 600 K [10] and goes up to above 1200 K for tungsten annealed at high temperature [11]. W is susceptible to embrittlement, i.e. the DBTT is rising by grain coarsening [12] or/and neutron irradiation [13,14].

Tungsten fibre-reinforced tungsten composites W_f/W utilize extrinsic mechanisms to improve the fracture toughness. The brittleness problem of W is thereby mitigated and an application as a plasma facing material under thermal transients and neutron bombardment becomes feasible. A similar approach has been successfully applied to ceramic materials reinforced by ceramic fibres for many years [15].

W_f/W composites consist of tungsten fibres made of commercially available tungsten wire embedded in a tungsten matrix produced either by a chemical process [16,17] or by powder metallurgy [18]. In the past years, it has been shown at the Max-Planck-Institute for Plasma Physics, Garching (IPP) that extrinsic toughening can be achieved in such composite systems [19,20]. Being a key factor for the effective operation of this toughening mechanism the interface between fibre and matrix was investigated in a first step [21,22]. Engineered layers provide a stable interface during production and operation. Model systems consisting of a single W fibre embedded in a chemically deposited tungsten matrix were used to prove the feasibility of the toughening effect. It was shown that various extrinsic toughening mechanisms, e.g. fibre bridging, fibre pull-out etc. are active in the as-fabricated case as well as after embrittlement of the fibre by recrystallization and grain growth[1] [20]. In addition it was shown that the plastic deformation of the fibre makes an important contribution to the toughening in the as-fabricated state [23]. In a further development step a fabrication method for bulk material based on the chemical deposition of W was developed and first samples were produced. Mechanical tests on these samples revealed an intense toughening at room temperature and active toughening mechanisms in embrittled conditions. Based on these results the material was chosen as risk mitigation plasma-facing component and high heat flux material in the EU Fusion roadmap [2,3].

In [24] we presented a development approach towards the use of W_f/W in a future fusion reactor. As a first step components will be fabricated and tested under high heat flux conditions. The components will be designed according to the ITER reference design of small-scale divertor mock-ups [25]. High heat flux testing of small scale mock-ups is a well-established method to qualify material for the use in a fusion divertor and is for example used in the ITER qualification program. Two designs are very common: a so-called monoblock design where the whole component consists of the plasma facing material connected to a cooling tube in the central region, and a flat tile design where a plate of this material is connected to a larger cooling structure [26].

In this article we present a way to utilize W_f/W composites for divertor applications by a fabrication route based on the chemical vapour deposition (CVD) of tungsten. A technique to produce W_f/W material which can be used for producing monoblock or flat tile mock-ups is introduced and mechanical test results of such material showing increased fracture energy are shown. In addition we address the benefits of such a material system and present new techniques/methods for improving the manufacturing process.

2. Divertor mock-up components made of W_f/W

Based on the mock-up design presented by Hirai et al. [25] a possible W_f/W mock-up is shown in Fig. 1. The mock-up is made of 5 segments attached to a CuCrZr cooling tube. The single segments consist either of W_f/W only (monoblock) or of a W_f/W plate attached to a *Cu* structure. In the following we present a possible fabrication approach for such mock-ups together with first results. For a flat tile design W_f/W tiles with a thickness of 5 mm are needed. For a monoblock design tiles with a thickness of 12 mm are used in an upright position. The geometry including the necessary hole in the monoblock case are produced by spark erosion. In the case of the flat tile concept the W_f/W parts are connected to the Cu structure by brazing [27]. Finally the segments are joint with the cooling tube by hot radial pressing [28] (monoblock) or again brazing (flat tile). In both cases the W_f/W tiles are arranged in a way that the fibres will be orientated parallel to the surface.

2.1. W_f/W tile by layered deposition process

First W_f/W tiles have been produced utilizing a layered deposition procedure. In this process the tile is produced by successive chemical vapour deposition (CVD) of W on single layers of equally distanced and unidirectional orientated tungsten wire with a diameter of 150 μm (similar wire has been used for the chemical infiltration experiments performed in [16]). These layers are produced in a multi step process. First the wire is wound around a frame consisting of two fine threaded top ends in a way that the distance between the wire is determined by the pitch (500 μm in this case). This results in a top and bottom layer of wire pieces (called fibres in the following) with a free distance of 350 μm between each other. By a vertical adjustable clamping system the two layers are brought into one plane and the distance of the fibres is adjusted to the final distance of 100 μm.

To form the composite a fibre layer is placed on a heated surface where the applied process gas (WF_6 and H_2) reacts in a surface reaction to form W deposit which starts to ingrow the layer. After reaching the required thickness for the desired vertical layer distance the already ingrown layer is cut free of the frame. Then a second fibre layer is placed on top and is ingrown again. This procedure is repeated until the desired sample height is reached. By this procedure a vertical distance of the fibre layers slightly above 100 μm is achieved. The footprint of the final sample is determined by the size of the used fibre layer and the height is determined by the number of layers put on top of each other. The resulting fibre volume fraction is up to 30% (depending on the vertical distance between the individual fibre planes). To provide a stable interface to the matrix the fibres are typically coated by magnetron sputtering e.g. by an Er_2O_3 interface layer with a thickness of 1 μm (see [19] for details of the process) prior to the matrix production.

Samples with a footprint of 50 by 50 mm^2 containing up to 10 fibre[2] layers have been produced so far (see Fig. 2). The samples thickness varied between 3.5 and 4 mm and the density reached 94% (determined by Archimedes principle). Microstructural investigations revealed that the deposition itself was very dense (no micropores) and that large pores were formed in between the fibres by premature stopping of the deposition due to pore blocking. This was especially a problem if the fibres were not well arranged and thus a large variety of different distances between the fibres was

[1] This condition is called “embrittled” in the following.

[2] The fibres were coated by an Er_2O_3 interface layer with a thickness of 1 μm.

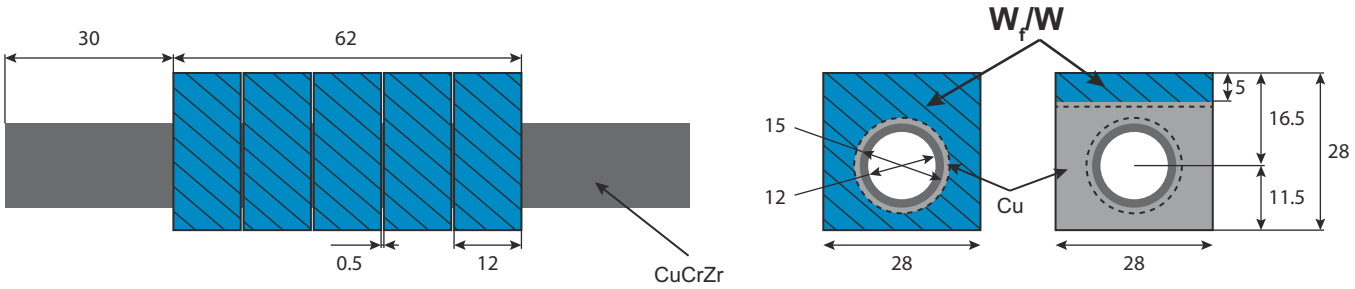

Fig. 1. A Mock-up based on a monoblock and flat tile concept utilizing W_f/W composites. The design is according to the small scale mock-ups used for the ITER qualification program [25]. On the left hand side the whole mock-up is shown in a side view. 5 segments are connected to a CuCrZr cooling tube. A front view of such a segment is shown for both monoblock and flat tile design on the right. For the monoblock design the whole segment consists of W_f/W for the flat tile design a W_f/W plate is attached to a Cu structure.

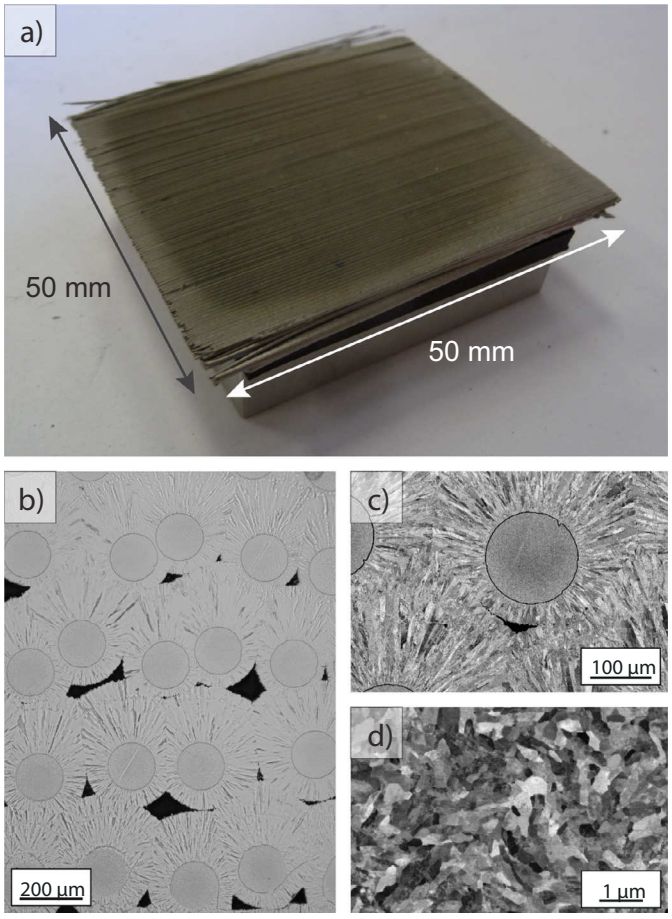

Fig. 2. W_f/W composite produced by a layered deposition process. In (a) a photo of the full sample is shown. (b) shows a light microscopy picture of the cross-section. Large pores in between the fibres are clearly visible as well as regions with high density. In (c) and (d) scanning electron microscopy pictures show the microstructure in detail. In (c) the star like growing grain structure of the matrix is shown. (d) shows a close up of the fibre centre with the remaining very fine grain structure. (Note that pictures (b-d) are showing details of (a) but not the same cross-sections.)

present. This was true for variations within a layer as well as between layers. However, almost pore free deposition was possible in areas with uniform fibre distances.

2.2. Charpy impact test

Charpy impact testing, standardised in ASTM E23 [29], allows the determination of the fracture energy and thus gives indication of the toughness. In addition such tests conducted at various temperature are used to determine the ductile-to-brittle transition temperature (DBTT). For materials with restricted availability miniaturized samples of the so called KLST (from the German "Kleinstprobe") type geometry are frequently used [30]. These type samples have been used for tungsten materials before and allow therefore a good comparability [31,32].

To investigate the fracture toughness of W_f/W composites Charpy impact tests were conducted at room temperature. KLST type samples were produced out of a W_f/W-plate produced by layered deposition process described above. The sample dimensions were 27 mm × 3 mm × 4 mm with a 1 mm deep notch. The specimens were prepared in a way that the fibres are perpendicular to the loading direction. Regarding the growing direction during the CVD process the sample was grown in width direction. The samples including the notch were machined by spark erosion and then polished to the final dimensions. 5 samples have been produced and tested. The fibre volume fraction was determined after the test by SEM investigations of the fracture surface to be around 20% (only complete fibres are considered) (see Table 1). The pendulum height was 0.74 m which results in a velocity of 3.81 ms^{-1} when the mass hits the sample.

The results are summarized in Table 1. The Charpy energy varies between 0.64 J and 0.88 J. The fracture surface was investigated by means of electron microscopy after the test. In Fig. 3 a typical fracture surface is shown. The matrix shows brittle failure with a mixture of cleavage and intergranular fracture. In general almost all fibres failed ductile by necking and knife edge failure of individual grains. The reduced cross-section after the test is measured for some fibres (8 fibres of 1 sample) and gives a reduced diameter of 102 ± 2 μm (the error is calculated as standard deviation of the mean). Only a minor fraction (≤ 7% depending on the sample) of the fibres show brittle fracture. Some fibres did not fracture during the test (see Table 1 and Fig. 3). In addition some delamination between fibre layers (formed by the stepwise fabrication process) was observed in sample 4 and 5.

Due to the brittle behaviour of the W matrix linear elastic fracture mechanics can be applied for a first estimation of the fracture toughness K_c using the above reported results and following relation (assuming plane strain condition) [33]:

$$K_c = \sqrt{\frac{G_c E}{1-\mu^2}} = \sqrt{\frac{U_f E}{A(1-\mu^2)}} \quad (1)$$

with	G_c : critical energy release rate	[N m^{-2}]
	E : Young's Modulus of W	[400 GPa]
	μ : Poission's ratio	[0.3]
	U_f : fracture energy	[J]
	A : fractured area	[m^2]

Besides the real fracture en energy U_f, the kinetic energy (used to accelerate the specimen) and the energy used for the elas-

Table 1
Overview of Charpy impact test results. The uncertainties are calculated as standard deviation of the mean.

	Dissipated energy U [J]	*Dissipated energy per area* [J mm^2]	*Fibre volume fraction* [-]	*Unbroken fibres* [%]	*Brittle fibres* [%]
1	0.83	0.092	0.21	6	2
2	0.78	0.093	0.21	5	0
3	0.64	0.069	0.20	5	2
4	0.88	0.104	0.19	9	2
5	0.73	0.077	0.19	10	0
	0.77 ± 0.04	0.09 ± 0.01	0.20	7	1

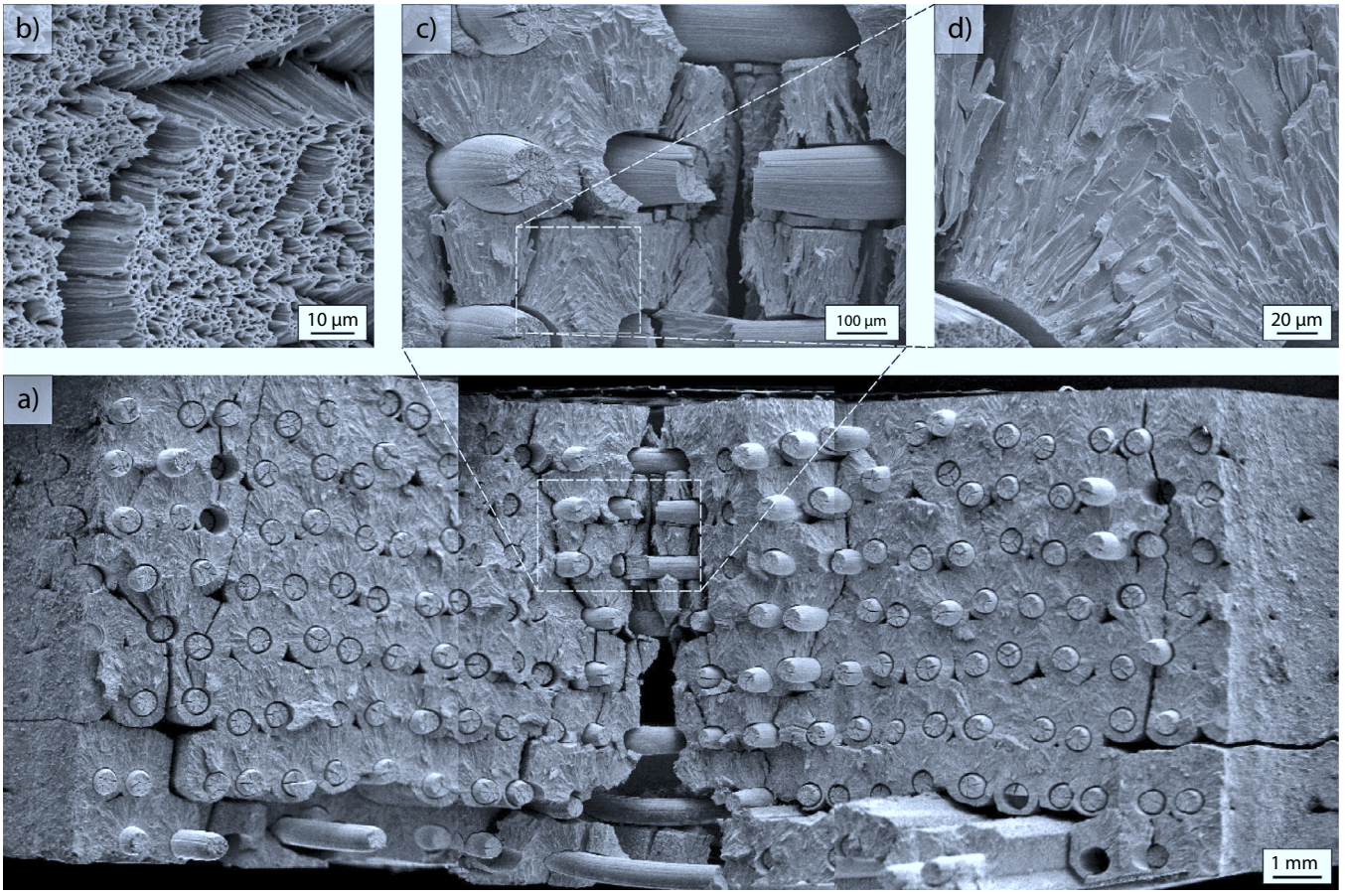

Fig. 3. Typical fracture surface of a W_f/W sample after a Charpy impact test (a). The close-ups (c+d) show a typical region of the matrix fractured in a mixture of cleavage and grain boundary failure and a necked fibre with a knife-edge like fracture (b).

tic deformation of the testing machine are main contributions to the measured Charpy energy U [34]. Based on experiments of Kobayashi et al. [35] on ceramics where the U_f is between 0.4U and 0.6U a ratio of $U_f/U = 0.5$ is assumed for the calculation of K_c in this case. A mean value of $K_c = 140 \pm 5\,\mathrm{MPam}^{0.5}$ is calculated (error is given as the standard deviation of the mean). The applicability of this method and the classification of the determined value is discussed in Section 5.

3. Benefits of a W_f/W-based divertor mock-up

3.1. Temperature window

Materials used in a fusion reactor feature different optimal operation temperature, their so-called temperature window. Fig. 4 shows the temperature windows for several materials for a possible application in the divertor region. Tungsten is shown in comparison to typical cooling structure materials like Cu and steel. It is important to notice that up to now there is a gap between the operation temperature of the typical cooling structure materials and tungsten. In a component utilizing both material as e.g. shown in Fig. 1 this is a severe problem as one or the other or both materials have to be operated in an unfavourable temperature regime.

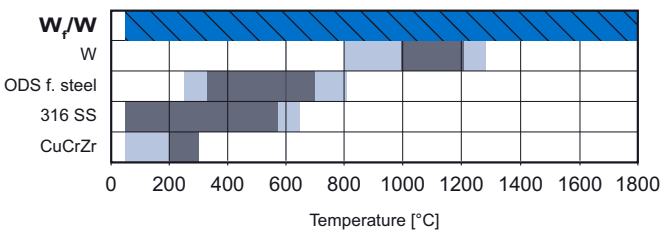

Fig. 4. Typical optimal temperatures for different materials foreseen to be used in the divertor in comparison to a possible temperature window of W_f/W. The data for W and the steels are based on [37], the data for CuCrZr is based on [60]. The dark grey areas mark the region of the optimum operation temperature. In the light grey areas operation is still possible. A potential operation temperature window of W_f/W is shown on the top.

The mechanical properties play a key role for the optimum operation temperature of tungsten. The lower boundary of the operation temperature is determined by its inherent brittleness [36] and low temperature irradiation embrittlement [37]. The upper temperature limit is given by the recrystallisation temperature above which the mechanical properties like strength and ductility deteriorate significantly [38]. In addition irradiation effects e.g. radiation enhanced recrystallisation or radiation creep play an important role.

In the case of W_f/W the incorporation of W fibres facilitates mechanisms of energy dissipation and thus an increased toughness (see Section 1 for more information). Various mechanisms are active at which the main mechanisms are the pure elastic effects of crack bridging and pull-out and, in the as-fabricated case, the ductile deformation of the fibre [24,39]. These mechanism provide a high toughness even at room temperature although the CVD matrix material itself is brittle (see Section 2.2). The lower operation temperature is therefore extended down to room temperature. Even if the fibres loose their ductility due to low temperature irradiation the elastic mechanism remain active and provide a significantly enhanced toughness [17]. The upper temperature border can be moved up to 1800 °C by utilizing potassium doped W wire which shows an exceptional stability against temperature induced embrittlement [24] as well as an excellent high temperature strength [12] and creep resistance [40]. Similar to the low temperature case the elastic mechanisms provide an enhanced toughness even if the fibre properties are degraded by irradiation effects.

Based on the up to now available experimental results a potential operation temperature window for W_f/W is shown in Fig. 4. Open questions and research needs regarding this zone are discussed in Section 5.

3.2. Suppression of crack growth

Deep cracking has been observed in small or medium scale W monoblock divertor mock-ups at high heat flux testing with slow transients of 20 MW m^{-2} [38]. Recently, Li and You [41] presented a theoretical interpretation of this phenomenon by finite element modelling (FEM). They identified low cycle fatigue failure as the most probable reason for crack initiation. Due to strong crack tip opening loads cracks can evolve deeply in a brittle manner when the crack grows into a large crack.

In W_f/W extrinsic mechanisms allow the reduction of stress peaks at crack tips and thus increase the resistance against the crack propagation. To get first insight into the effect of extrinsic toughening on this deep cracking phenomenon the effect of intact fibre layers on the driving force of the crack propagation was investigated. For this a static situation with a precrack similar to the real situation was assumed.

Therefore the FEM model described in [41] was complemented by two layers of W fibres and a pre-crack of 3 mm length was defined in a recrystallized W layer at the top of the tile (compare Fig. 5). To keep the computational cost at an acceptable level tungsten fibres with a radius of 250 μm and an overall fibre volume fraction of 13% was assumed in the precracked area. The fibres are assumed to behave purely elastically. No cracks in the fibres are allowed and a debonding length of 250 μm starting from both crack surfaces was assumed for all fibres. Further simulation setups can be found in the previous work. Fig. 5 shows the stress distribution in x-direction after high heat flux load of 20 MW m^{-2} (sample temperature 100 °C). The tensile stress which is the driving force for the crack propagation is limited in a small area in the vicinity of the pre-crack tip. The tensile stress in the fibres is relatively high and reaches 2400 MPa in the central region of the upper fibre layer.

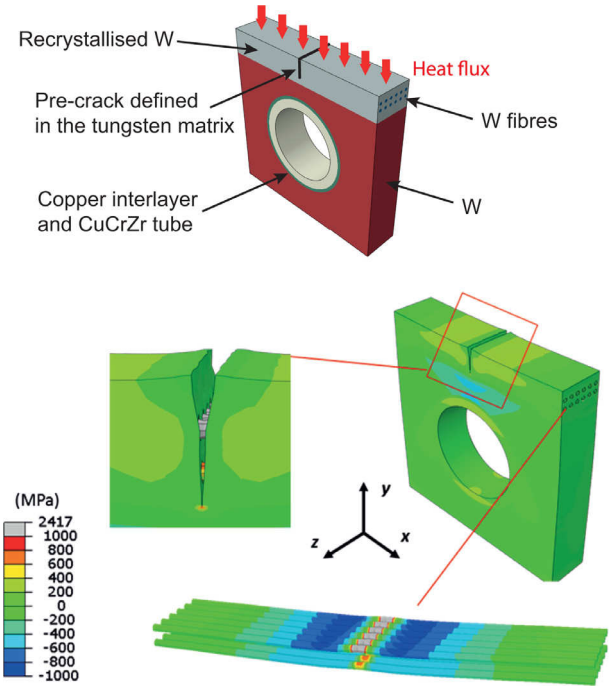

Fig. 5. Upper picture shows FEM model described by Li and You [41] complemented by two layers of tungsten fibres and a precrack of 3 mm. In the lower part the stress distribution in x-direction after a high heat flux load of 20 MW m^2 calculated by FEM is shown. The crack region and the fibres are shown in detail.

The J integral is a measure of the energy release rate G of a crack in non-linear elastic materials [42]. If its value is larger than a critical value, which is the materials resistance to crack propagation and thus fracture toughness, a crack propagates. The J-integral was calculated for the case with and without the tungsten fibre layers after the component was cooled down to the assumed coolant temperature of 100 °C. The critical value is calculated from fracture toughness of tungsten at 400 °C [43] to be 0.25 mJ mm^{-2}. In the case without fibres the J integral is calculated to be 3.25 mJ mm^{-2} and thus 13 times higher than the critical value. For the case with fibres the value is 0.20 mJ mm^{-2} and thus lower than the critical value.

4. Advanced composite fabrication methods

4.1. Tungsten fibre fabrics

For the layered deposition concept presented in Section 2 fibre layers having a unidirectional fibre arrangement with a defined distance between the fibres are needed. In the current experimental state a mostly manual process route is used to produce such layers (see Section 2.1 for details). Due to the many process steps and the lack of automation this procedure is time consuming and not very flexible.

As an improvement of this issues the application of textile techniques for W wire was evaluated. Tungsten fabrics were produced with a Mageba shuttle loom (typeSL) weaving machine. As a first step the tungsten wire was rewound on smaller spools which are more suitable for the weaving process in a rewinding machine Herzog USP 300 Electra. To avoid excessive twisting of the wire deflection spools were dismounted before the rewinding process. The fabric was then woven with a plain weave pattern using a DERIX350/10 reed and 60 tungsten wires. The warp wires were tungsten wires with a diameter of 150 μm and a warp wire distance of 100–150 μm. The weft wire were tungsten wires with a diameter of 70 μm and the weft wire distance was varied from

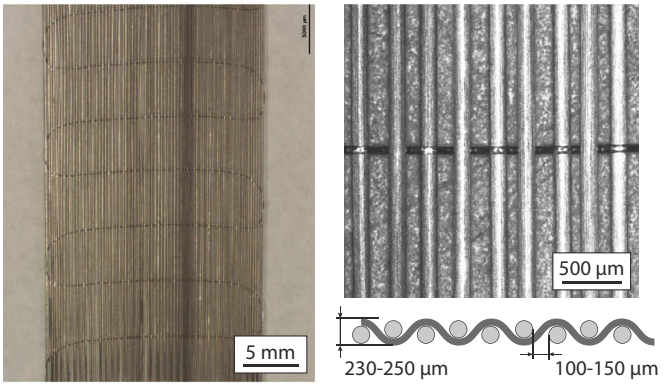

Fig. 6. Tungsten wire plain weave fabric with 150 μm diameter warp wires and 70 μm diameter weft wire. A small defect in the used reed leads to a smaller distance between the warp wire in a small region (darkish stripe). The warp wire distance is between 100 and 150 μm and a the thickness between 230 and 250 μm (see close up on the right).

30–50 mm. With this weaving set up it is possible to produce a 15 mm wide pure tungsten fabric with a thickness of 370 μm (caused by the fact that the weft wire is between two warp wires). By compression the weft wire is bent and a final thickness of 230–250 μm is reached.

The resulting fabric is shown in Fig. 6. A relatively uniform warp wire distance is achieved. Still some weaving errors are present. They mainly occur at the outer parts of the fabric where the weft wire pulls the fabric together but is too stiff to follow the shuttle in the desired way.

4.2. WILMA – W infiltration machine

The chemical vapour deposition of tungsten was frequently used for the production of W_f/W [16,17] as it allows low processing temperatures and a force-free production. The used process is the heterogeneous surface reaction of WF_6 and H_2 to form a solid W deposit and gaseous HF.

$$WF_6(g) + 3H_2(g) \longrightarrow 600\ \mathrm{K} - 1100\mathrm{K}W(s) + 6HF(g) \qquad (2)$$

Both, surface processes [21] (chemical vapour deposition CVD) as well as infiltration processes [16] (chemical vapour infiltration CVI) are utilized. It was shown in these experiments, that for the production by chemical processes the optimum pressure range is between 1–100 mbar and a maximum flexibility should be available for gas flow and temperature control.

Based on these results the device WILMA (**W** Infi**L**tration **MA**chine) was developed to meet these requirements and allow the surface deposition or infiltration of W on different surfaces and preforms. The deposition is conducted in a bell-shaped vacuum chamber with a diameter of 500 mm and a height of 750 mm. Inside this vessel the individual experimental setup is placed. A setup consists generally of a specially designed sample holding system. As the system is operated as a cold wall reactor[3] the setup typically includes also a local heating system. Depending on the desired deposition mode (surface or infiltration) gas guiding devices can be installed allowing different transport mechanisms, e.g. diffusion only or diffusion and convection.

As CVD or CVI experiments for W_f/W are mostly conducted at low pressure conditions, a liquid ring pump and a booster pump are placed at the exhaust as well as a valve for the pressure regulation. The system allows operation in a pressure window of 1–100 mbar.

[3] The walls are kept to a moderate temperature (around 200 °C in order to avoid condensation of the process gases on the vessel walls.

The vessel has several inlets, where pressure transducers, thermocouples or heating elements can be attached or inserted into the vessel. Furthermore, there are three inlets for gases at the vessel, two for the reacting gases, WF_6 and H_2, and one for argon for the possibility to purge the whole vessel properly between the experiments. The gas flow of the three gases is regulated with flow controllers. All parts of the facility are connected to a control system, which allows fully automatic operation by regulating pressure, temperature and gas flow. As highly toxic hydrofluoric acid is the end product of the reaction, the exhaust gas is neutralized by NaOH solution.

4.3. Modelling of infiltration process

Process understanding and predictability are important aspects in the optimisation of W_f/W fabrication by chemical processes. Modelling of the transport as well as the deposition processes allow an estimation of the optimum deposition parameters.

As the dissociation of the H_2 molecule is reported to be the rate determining step, the modelling of the hydrogen transport allows to get insight into the process. An analytical solution for the filling of a cylindrical pore as a model system has been presented by Riesch [20]. The model describes the influence of the transport by convection and diffusion and of the chemical reaction on the concentration as well as the change of geometry by the deposition. The deposition rate and therefore the uniformity of the process as well as the amount of reacted gas are calculated. The inclusion of the influence of temperature, gas flow and pressure as well as the initial pore size allows for detailed parameter studies. The following two differential equations describe the process:

$$\begin{aligned} \frac{dc_{H_2}}{dt} &= \overbrace{-D\frac{d^2c_{H_2}}{dx^2}}^{\text{diffusion}} + \overbrace{u_x\frac{dc_{H_2}}{dx}}^{\text{convection}} + \underbrace{S_V \cdot k_{H_2} \cdot {c_{H_2}}^{1/2}}_{\text{deposition/consumption}} \\ & \qquad \underbrace{\qquad\qquad\qquad\qquad}_{\text{mass transport}} \\ \frac{dS_V}{dt} &= f(c_{H_2}, T) \end{aligned} \qquad (3)$$

with	c_{H_2} : concentration H_2	[mol m^{-3}]
	D : diffusion coefficient H_2	[m^2 s^{-1}]
	u_x : gas velocity in x-direction	[m s^{-1}]
	S_V : surface per volume increment	[m^2 m^{-3}]
	k_{H_2} : rate constant H_2 consumption	[mol s$^{-1}m^{-0.5}$]

The first equation describes the concentration change of H_2 by mass transport and the consumption of H_2 due to the W deposition. The factor $k_{H2} \cdot {c_{H2}}^{1/2}$ links the consumption of H_2 to the deposition of W. The second equation describes the change of the geometry due to the deposition of W.

The most important assumption in this model is the dissociation of the H_2 molecule as rate determining step. This is valid if there is a reaction limitation rather than a transport limitation. This is the case if only a minor fraction of the transported gas actually reacts (gas excess). As the mass transport gets lower with decreasing pore radius and simultaneously the consumption increases the transport limitation is becoming more important if the pores get thinner. Calculations have shown that this is not the case until the pore radius reaches 5 μm and the gas flow is larger than 0.1 mol m^{-2} s^{-1}.

Provided that the above mentioned conditions are fulfilled the main results are that the concentration gradient induced by the convection results in an inhomogeneous pore filling. By decreasing the forced flow the concentration gradient is decreasing and the deposition gets more uniform. The temperature on the other hand only governs the deposition rate and as long as there is enough reaction gas available it has little effect on the homogeneity of the deposition but a large effect on the duration until the pore is

filled. New results indicate that the concentration gradient caused by the convectional flow might be overestimated in the current model.

5. Discussion

5.1. Fabrication process

The layered deposition process provides a technique for the production of bulk W_f/W in sizes suitable for a divertor mock-up application. Compared to the up to now used infiltration techniques [16,44] this process is mostly a surface process with a very shallow infiltration depth (around 150 μm, governed by the height of one fibre layer). Therefore the gas transport is higher and it is easier to control the process in a way to ensure the chemical reaction as rate limiting step. This allows higher process pressures and therefore higher deposition rates. For full scale mock-ups the deposition thickness needs to be enhanced by a factor of 1.5 for a flat tile design and a factor of 4 for a monoblock design. This can be reached by putting more fibre layers on top of each other without any new technological challenges.

A main reason for the remaining porosity originates from non-uniformities of the fibre arrangement. Woven tungsten fabrics feature a high uniformity and can therefore provide a solution. The use of tungsten fabrics will also decrease the complexity and duration of both the preform production and the deposition process. An adaptation of the weft wire density allows the production of 2D structures. For lowering the process time and more important to avoid internal interfaces the deposition process should be done continuously. This requires more advanced deposition setup developments. The high availability and flexibility provided by the new device WILMA will allow for the necessary parameter range and testing resources.

This new possibilities will also allow to improve the infiltration process. Preforms for infiltration processes can now readily be produced by using W wire fabrics. This will be much faster and easier compared to the so far used winding process [20]. The model presented in Section 4.3 can assist in the optimization of the infiltration process and similarly also in the optimisation of the layered deposition process. An important aspect is the adoption of the model being able to describe the complete filling of pores (below 5 μm).

5.2. Charpy impact test

Charpy impact test were conducted on samples produced by the above discussed layered deposition approach. The quality of the samples regarding porosity and internal interfaces is important. The observed delaminations are probably caused by internal interfaces caused by the stepwise fabrication process. Pores on the other hand could act as crack stopper and falsify the results.

All 5 tested samples show a brittle fracture in the tungsten matrix and accordingly a low Charpy energy. However these values are higher than values obtained for pure tungsten and tungsten alloys up to 300 °C (similar geometry and testing procedure) [11,45]. They exceed the values obtained for TZM (molybdenum, stabilized by Ti and Zr) at room temperature [46]. Tungsten foil laminates (W content $\approx$ 50%) show an approximately 2 times larger value at room temperature [31]. A reason for that can be the higher content of the ductile phase foils (50%) compared to the wire in W_f/W (20%).

The brittle fracture in the chemically deposited matrix shows a mixture of grain boundary failure and cleavage typical for tungsten at room temperature [9]. This was reported for chemically deposited tungsten [47] and W_f/W composites [16,23] before. The fibres however show almost all the typical ductile failure of tungsten wire caused by grain boundary delamination followed by knife edge failure of single grains [39,48]. The necking induced reduced diameter of 102 $\pm$ 2 μm is in the same range as the values observed for free fibres (113 μm) [39] and constraint fibres (114 μm) [23]. Assuming the diameter reduction as a measure of ductile deformation higher testing speed even seems to be beneficial which is in fact counter-intuitive from previous results on fracture toughness [49,50].

As the tests were conducted only at room temperature they do not allow to determine a distinct DBTT but nevertheless give some indications. The ductile failure of nearly all fibres is a clear indication that the ductile to brittle transition temperature is below room temperature for the used tungsten wire. The DBTT for the chemically deposited tungsten matrix is clearly at higher temperature. Tests at elevated and lower temperature should be conducted to determine the respective temperature for wire and matrix. As the mechanical properties of the CVD matrix material are strongly influenced by the deposition parameters (determines grain size and grain orientation) [51] or/and possible impurities [47] special care is needed for the sample fabrication.

A first calculation approach for the fracture toughness has been presented. The ductile deformation of the fibres is described as the main contribution in the as-fabricated state of W_f/W and can therefore give insight into the validity of the approach. For the fully ductile fracture within W_f/W Riesch et al. [23] give an energy consumption for a single fibre of 3.4 mJ. Assuming the same energy to be consumed by each fibre in the Charpy test an approximation of the contribution by plastic deformation to the overall fracture toughness of $\Delta G_{pl} = 0.035\,\mathrm{Jm}^{-2}$ corresponding to a contribution to the crack intensity factor of $\Delta K_{pl} = 124\,\mathrm{MPa\ m}^{0.5}$ (using Eq. 1). This shows that the plastic deformation has a huge impact on the overall fracture energy. Assuming that due to its brittle nature the matrix only plays a minor role, it also proves that the applied calculation of the fracture toughness is reasonable (compare Section 2.2).

Nevertheless it has to be considered that geometry effects [33,52] as well as size effects [53] are reported to play an important role in the correlation of Charpy energies and fracture toughness. Zhang and Shi [54] describe a similar method where the energy consumed up to the maximum load point is used to calculate the fracture toughness according to Eq. 1. Here it is important to differentiate between purely brittle material like ceramic or material able to provide plasticity like steels. Looking at the load curves of brittle materials e.g. presented by Kobayashi et al. [35] this energy corresponds to the overall measured energy as these materials fail completely after a fully elastic loading. In the case of W_f/W this is true for the matrix material however the fibres could have an impact after crack initiation. An approach e.g. suggested by Schindler [55] or Schneider [56] will be used for the further interpretation of the results and for the design of further experiments. Instrumented Charpy impact tests could provide more information (see for example [35,54,57]) in this respect.

5.3. Fracture toughness

The main assumption of the presented calculation approach for the fracture toughness is that linear fracture mechanics are applicable for W_f/W which seems reasonable as the matrix of the material behaves brittle without any plastic contribution (see above description). The contribution of the fibre ductility acts behind the crack tip and thus lowers (by dissipation) the crack driving energy rather than directly influencing the matrix material at the crack tip. The following equation describes this relation:

$$G - \Delta G \begin{cases} < G_{c,\mathrm{matrix}} & \Rightarrow \text{crack halts} \\ > G_{c,\mathrm{matrix}} & \Rightarrow \text{crack propagates} \end{cases} \quad (4)$$

with	G : energy release rate for crack driving
	ΔG : consumed energy by extrinsic mechanisms
	$G_{c,matrix}$: critical energy release rate of matrix

The most important aspect here is that the enhanced toughness is not linked to an improvement of the material itself (intrinsic toughening) but is induced by mechanisms introduced by the fibres (extrinsic toughening). Consequently, as long as the mechanisms are active it does not matter if the actual material gets degraded. This was shown by Riesch et al. [23] for model samples and by Neu et al. [17] for bulk material. In these investigations the fracture toughness could be significantly improved by mechanisms not relying on any material plasticity. Another example for this mechanism are ceramic fibre reinforced ceramics which show a superior fracture toughness although their constituents are fully brittle [58,59].

For this reason extrinsic toughening allows to overcome the brittleness problem of W and especially the problem of embrittlement during operation. As presented in Section 3.1 the use of W_f/W could therefore bridge the temperature window gap between heat sink material and plasma facing material. However so far only first tests at room temperature have been conducted on non-standardized samples. A material qualification program is necessary to prove the desired properties for relevant geometries and loading conditions as well as in the desired temperature range. Finally tests of irradiated material have to prove that the same mechanisms are valid after neutron induced embrittlement. Looking at the constituents potassium doped tungsten wire is known for its excellent high temperature strength. However mechanical tests were only conducted for annealed samples so far. Test at elevated temperature are indispensable to determine the operational constraints.

In Section 3.2 the resistance to crack propagation in W_f/W, i.e. fracture toughness, was investigated for foreseen geometries and loading cases by FEM simulations. Compared to existing W_f/W samples the fibre volume fraction is smaller and the fibre diameter is larger. In addition the only extrinsic effect considered in the calculations so far is elastic bridging. Despite these simplifications the assumed (pre-) crack is stopped. Increasing the fibre volume fraction to 20% (compare Section 2) or even larger would improve the gain in fracture toughness as the elastic bridging scales linearly with the bridging area (and this in turn with the fibre volume fraction). The consideration of other toughening mechanisms like plastic deformation or pull-out would further improve this gain. The observed stress in the fibres is very large but strength values of this level have already been proven for potassium doped wire at room temperature [24].

6. Conclusion and outlook

W_f/W composites show toughness in the as-fabricated and in embrittled conditions. Elaborating this composite material to a divertor mock-up element will allow the improvement of the operation temperature window and suppress cracking problems. By using a layered CVD process plates with sufficient dimensions can be produced. In Charpy impact tests increased fracture energy mainly due to the ductile deformation of the tungsten fibres was shown at room temperature. Advanced methods like the application of textile techniques, a new deposition device, and modelling respectively, allow the improvement of the fabrication process. The main conclusions are:

- The production of small-scale mock-ups based on W_f/W composites suitable for high heat flux tests is feasible using existing techniques. An improvement in quality and the industrial up scaling is ensured by new methods.
- The DBTT of drawn tungsten wire (with a diameter of 150 μm) is below room temperature. This leads to an increased energy consumption in Charpy impact tests.
- The DBTT of chemically deposited W is above room temperature allowing the application of liner elastic fracture mechanics.
- Extrinsic toughening provides increased fracture toughness and thus solutions for the use of W in divertor applications.

A key factor is the behaviour of W_f/W at elevated temperature. Tests on bulk material as well as on the constituents -fibre and matrix- are foreseen. To get insight into the behaviour at irradiated conditions irradiation campaigns as well as comparison of temperature and irradiation embrittlement are planned. A further important aspect for the use of W_f/W in the divertor region is its behaviour in the fusion environment. Important aspect in this respect are e.g. thermal stability, activation, the interaction with hydrogen or physical erosion. This issues will be discussed in detail elsewhere.

Acknowledgements

The authors want to thank G. Matern and M. Balden for their assistance in microscopy. We acknowledge the discussion with M. Reinelt and K. Schmid about modelling. We thank the Osram GmbH, Schwabmünchen, Germany for providing the tungsten wire and Archer Technicoat Ltd, High Wycombe, UK for the CVD production. Furthermore, we want to acknowledge the Institute of Materials Science and Mechanics of Materials of TU Munich for performing the Charpy impact tests. This work has been carried out within the framework of the EUROfusion Consortium and has received funding from the Euratom research and training programme 2014–2018 under grant agreement No 633053. The views and opinions expressed herein do not necessarily reflect those of the European Commission.

References

[1] D. Maisonnier, D. Campbell, I. Cook, L.D. Pace, L. Giancarli, J. Hayward, A.L. Puma, M. Medrano, P. Norajitra, M. Roccella, P. Sardain, M. Tran, D. Ward, Nuclear Fusion 47 (2007) 1524–1532.
[2] F. Romanelli, Fusion Electricity – A Roadmap to the Realisation of Fusion Energy, European Fusion Development Agreement, EFDA, 2012. https://www.euro-fusion.org/wpcms/wp-content/uploads/2013/.
[3] D. Stork, P. Agostini, J. Boutard, D. Buckthorpe, E. Diegele, S. Dudarev, C. English, G. Federici, M. Gilbert, S. Gonzalez, A. Ibarra, Ch. Linsmeier, A. Li Puma, G. Marbach, P. Morris, L. Packer, B. Raj, M. Rieth, M. Tran, D. Ward, S. Zinkle, J. Nuclear Mater. 455 (2014) 277–291.
[4] R. Neu, ASDEX Upgrade Team, EU PWI Taskforce, JET EFDA Contributors, Plasma Phys. Control. Fusion 53 (12) (2011) 124040.
[5] G. Federici, R. Kemp, D. Ward, C. Bachmann, T. Franke, S. Gonzalez, C. Lowry, M. Gadomska, J. Harman, B. Meszaros, C. Morlock, F. Romanelli, R. Wenninger, Fusion Eng. Des. 89 (7-8) (2014) 882–889.
[6] C. Bachmann, G. Aiello, R. Albanese, R. Ambrosino, F. Arbeiter, J. Aubert, L. Boccaccini, D. Carloni, G. Federici, U. Fischer, M. Kovari, A. Li Puma, A. Loving, I. Maione, M. Mattei, G. Mazzone, B. Meszaros, I. Palermo, P. Pereslavtsev, V. Riccardo, P. Sardain, N. Taylor, S. Villari, Z. Vizvary, A. Vaccaro, E. Visca, R. Wenninger, Fusion Eng. Des. 98-99 (2015) 1423–1426.
[7] J. Coenen, S. Antusch, M. Aumann, W. Biel, J. Du, J. Engels, S. Heuer, A. Houben, T. Höschen, B. Jasper, F. Koch, A. Litnovsky, Y. Mao, R. Neu, G. Pintsuk, J. Riesch, M. Rasinski, J. Reiser, M. Rieth, B. Unterberg, T. Weber, T. Wegener, J.-H. You, C. Linsmeier, Phys. Scr. T167 (2016) 014002.
[8] M. Merola, F. Escourbiac, R. Raffray, P. Chappuis, T. Hirai, A. Martin, Fusion Eng. Des. 89 (2014) 890–895.
[9] C. Gandhi, M. Ashby, Acta Metall. 27 (1979) 1565–1602.
[10] E. Lassner, W.-D. Schubert, Tungsten – Properties, Chemistry, Technology of the Element, Alloys, and Chemical Compounds, Kluwer Academic/Plenum Publishers, 1999.
[11] J. Reiser, M. Rieth, B. Dafferner, A. Hoffmann, J. Nuclear Mater. 442 (2013) S204–S207.
[12] S. Yih, C. Wang, Tungsten: Source, Metallurgy, Properties, and Applications, Springer Science+Business Media New York, 1979.
[13] V. Barabash, G. Federici, M. Rödig, L. Snead, C. Wu, J. Nuclear Mater. 283–287 (2000) 138–146.
[14] J. Steichen, J. Nuclear Mater. 60 (1) (1976) 13–19.
[15] A. Evans, J. Am. Ceram. Soc. 73 (1990) 187–206.

[16] J. Riesch, T. Höschen, Ch. Linsmeier, S. Wurster, J.-H. You, Phys. Scr. T159 (2014) 014031.
[17] R. Neu, J. Riesch, J. Coenen, J. Brinkmann, A. Calvo, S. Elgeti, C. Garcá-Rosales, H. Greuner, T. Höschen, G. Holzner, F. Klein, F. Koch, Ch. Linsmeier, A. Litnovsky, T. Wegener, S. Wurster, J.-H. You, Fusion Eng. Des. (2016), doi:10.1016/j.fusengdes.2016.01.027.
[18] B. Jasper, J.W. Coenen, J. Riesch, T. Höschen, M. Bram, C. Linsmeier, Mater. Sci. Forum 825-826 (2015) 125–133.
[19] J. Du, A Feasibility Study of Tungsten-Fiber-Reinforced Tungsten Composites with Engineered interfaces, Technische Universität München, 2011 (Ph.D. thesis). http://mediatum.ub.tum.de/node?id=998317.
[20] J. Riesch, Entwicklung und Charakterisierung eines wolframfaserverstärkten Wolfram-Verbundwerkstoffs, Technische Universität München, 2012 (Ph.D. thesis). http://mediatum.ub.tum.de/node?id=1106428.
[21] J. Du, T. Höschen, M. Rasinski, S. Wurster, W. Grosinger, J.-H. You, Compos. Sci. Technol. 70 (2010a) 1482–1489.
[22] J. Du, T. Höschen, M. Rasinski, J.-H. You, Mater. Sci. Eng. A 527 (2010b) 1623–1629.
[23] J. Riesch, J.-Y. Buffiere, T. Höschen, M. di Michiel, M. Scheel, Ch. Linsmeier, J.-H. You, Acta Mater. 61 (19) (2013) 7060–7071.
[24] J. Riesch, Y. Han, J. Almanstötter, J.W. Coenen, T. Höschen, B. Jasper, P. Zhao, Ch. Linsmeier, R. Neu, Phys. Scr. T167 (2016) 014006.
[25] T. Hirai, F. Escourbiac, S. Carpentier-Chouchana, A. Fedosov, L. Ferrand, T. Jokinen, V. Komarov, A. Kukushkin, M. Merola, R. Mitteau, R. Pitts, W. Shu, M. Sugihara, B. Riccardi, S. Suzuki, R. Villari, Fusion Eng. Des. 88 (2013) 1798–1801.
[26] I. Smid, Mater. Sci. Forum 475–479 (2005) 1355–1360.
[27] C. Gualco, M. Grattarola, A. Federici, F. Mataloni, K. Izdinsky, F. Simancik, B. Schwarz, C. Garcia-Rosales, I. Lopez-Galilea, Adv. Mater. Res. 59 (2008) 192–197.
[28] E. Visca, C. Testani, S. Libera, M. Sacchetti, Fusion Eng. Des. 66–68 (2003) 295–299.
[29] ASTM E23-12c, Standard Test Methods for Notched Bar Impact Testing of Metallic Materials, ASTM International, West Conshohocken, PA, 2012, www.astm.org, doi:10.1520/E0023-12C.
[30] E. Lucon, C. McCowan, R. Santoyo, J. Splett, Special publication 260-180, National Institute of Standards and Technology, 2013.
[31] J. Reiser, M. Rieth, B. Dafferner, A. Hoffmann, J. Nuclear Mater. 423 (2012) 1–8.
[32] M. Rieth, A. Hoffmann, Int. J. Refract. Met. Hard Mater. 28 (2010) 679–686.
[33] H. Brown, J. Mater. Sci. 8 (1973) 941–948.
[34] T. Kobayashi, Strength and Toughness of Materials, Springer Japan, 2004.
[35] T. Kobayashi, M. Niinomi, Y. Koide, K. Matsunuma, Trans. Jpn. Inst. Met. 27 (10) (1986) 775–783.
[36] I. Smid, M. Akiba, G. Vieider, L. Plöchl, J. Nuclear Mater. 258–263 (1998) 160–172.
[37] Zinkle, N. Ghoniem, Fusion Eng. Des. 51-52 (2000) 55–71.
[38] G. Pintsuk, I. Bobin-Vastra, S. Constans, P. Gavila, M. Rödig, B. Riccardi, Fusion Eng. Des. 88 (2013) 1858–1861.
[39] P. Zhao, J. Riesch, T. Höschen, J. Almannstötter, M. Balden, J. Coenen, R. Himml, W. Pantleon, U. von Toussaint, R. Neu, Int. J. Refract. Met. Hard Mater. (2016). Submitted.
[40] H. Bildstein, R. Eck, High Temp. High Press. 10 (1978) 215–230.
[41] M. Li, J.-H. You, Fusion Eng. Des. 101 (2015) 1–8.
[42] T. Anderson, Fracture Mechanics: Fundamentals and Applications, Taylor & Francis Group LLC, 2005.
[43] B. Gludovatz, S. Wurster, A. Hoffmann, R. Pippan, Int. J. Refract. Met. Hard Mater. 28 (6) (2010) 674–678.
[44] J. Riesch, T. Höschen, A. Galatanu, J.-H. You, Proceedings of the Eighteenth International Conference on Composite Materials, Jeju, South Korea, 2011.
[45] M. Rieth, B. Dafferner, J. Nuclear Mater. 342 (2005) 20–25.
[46] M. Rieth, A. Hoffmann, Adv. Mater. Res. 59 (2009) 101–104.
[47] J. Murphy, A. Giannattasio, Z. Yao, C. Hetherington, P. Nellist, S. Roberts, J. Nuclear Mater. 386–388 (2009) 583–586.
[48] J. Leber, J. Tavernelli, D. White, R. Hehemann, J. Less Common Met. 48 (1976) 119–133.
[49] P. Gumbsch, J. Riedle, A. Hartmaier, H.F. Fischmeister, Science 282 (5392) (1998) 1293–1295.
[50] D. Rupp, S.M. Weygand, J. Nuclear Mater. 417 (2011) 477–480.
[51] H. Pierson, Handbook of Chemical Vapor Deposition (CVD) – Principles, Technology, and Applications, second, Noyes Publications/William Andrew Publishing, LLC, 1999.
[52] G. Marshall, J. Williams, C. Turner, J. Mater. Sci. 8 (1973) 949–956.
[53] H. Schindler, P. Bertschinger, in: I. Dlouhý (Ed.), NATO Science Series, vol. 78, Springer Netherlands, 2002, pp. 213–224.
[54] X. Zhang, Y. Shi, Int. J. Press. Vessels. Pip. 65 (2) (1996) 187–192.
[55] H.-J. Schindler, Mat.-wiss. u. Werkst. 32 (6) (2001) 544–551.
[56] H.-C. Schneider, Scientific Report FZKA 7066, Forschungszentrum Karlsruhe, 2005. http://bibliothek.fzk.de/zb/berichte/FZKA7066.pdf.
[57] G. Fearnehough, R. Nichols, Int. J. Fract. Mech. 4 (3) (1968) 245–256.
[58] K. Chawla, Ceramic Matrix Composites, Chapman & Hall, 1993.
[59] R. Jones, C. Henager Jr., J. Eur. Ceram. Soc. 25 (2005) 1717–1722.
[60] W. Timmis, Technical Report, Culham Centre for Fusion Energy, 2012.